




Assessing the effects of particle size and composition on light scattering through measurements of size-fractionated seawater samples

Daniel Koestner , * Dariusz Stramski , Rick A. Reynolds 

Marine Physical Laboratory, Scripps Institution of Oceanography, University of California San Diego, La Jolla, California

Abstract

Measurements of the particulate volume scattering function, $\beta_p(\psi)$, at light wavelength of 532 nm, particle size distribution, PSD, and several metrics of particulate concentration and composition were made on eight contrasting seawater samples from nearshore and coastal oceanic environments including river estuary and offshore locations. Both $\beta_p(\psi)$ and PSDs were measured on original (unfiltered) samples and particle size-fractionated samples obtained through filtration using mesh filters with pore sizes of 5 and 20 μm . We present results based on direct size-fractionated measurements and data adjusted for imperfect fractionation, which provide insights into the roles played by particle size and composition in angle-resolved light scattering produced by highly variable natural assemblages of aquatic particles. Despite intricate interplay between the effects of particle size and composition, small particles ($< 5 \mu\text{m}$ in size) consistently produced a major or dominant contribution ($\sim 50\text{--}80\%$) to the particulate backscattering coefficient, b_{bp} , in organic, either phytoplankton or nonalgal, dominated samples regardless of significant variations in PSD between these samples. The notable exception was a sample dominated by large-celled diatoms from microphytoplankton size range, which exemplifies a scenario when large particles ($> 20 \mu\text{m}$) can produce a considerable contribution ($\sim 40\%$) to b_{bp} . We also observed a trend for inorganic-dominated samples exhibiting consistently lower contributions ($\sim 30\text{--}40\%$) of small particles to b_{bp} . The particle size-based budget for the particulate scattering coefficient, b_p , indicates a significant decrease in the role of small particles accompanied by an increase in the role of larger particles compared to the b_{bp} budget.

The angular distribution of light scattered by natural waters has wide-ranging significance and potential applications in aquatic sciences, especially in oceanography. One of the most fundamental inherent optical properties (IOPs) of seawater is the spectral volume scattering function, $\beta(\psi, \lambda)$ (in units of $\text{m}^{-1} \text{sr}^{-1}$), which describes the scattered intensity at light wavelength, λ , as a function of scattering angle, ψ , per unit incident irradiance per unit volume of water (Mobley 1994). Integrating $\beta(\psi, \lambda)$ over all scattering directions gives the spectral scattering coefficient, $b(\lambda)$ (m^{-1}). In this integration, it is commonly assumed that light scattering by an assemblage of randomly oriented scatterers (molecules and particles) in natural waters is azimuthally symmetric about the direction of incident light beam. Similarly, integration within the range of backward scattering angles yields the spectral backscattering coefficient, $b_b(\lambda)$ (m^{-1}). It is common to include a subscript p in the notation of these inherent scattering properties (and other IOPs) to denote the contribution only by

particles in suspension with the contribution of molecular water (subscript w) removed, e.g., $\beta_p(\psi, \lambda) = \beta(\psi, \lambda) - \beta_w(\psi, \lambda)$. As the scattering measurements in this study were made at a single wavelength of 532 nm, we omit λ for brevity hereafter unless otherwise noted.

Because light propagation through the water column depends on scattering, radiative transfer simulations require the input data of the volume scattering function, $\beta(\psi)$, or scattering phase function, $\tilde{\beta}(\psi)$ which is typically defined as $\beta(\psi)$ normalized by b . Such simulations have been used to study numerous problems of ocean optics (Gordon et al. 1975; Mobley et al. 2002; Li et al. 2014) and have also been included in ocean biogeochemical and ecosystem models (Gregg 2002; Mobley et al. 2015). The effect of the angular shape of $\beta(\psi)$ has been explicitly incorporated in an ocean color analytical model, which has the potential for improvements of satellite remote sensing applications (Zaneveld 1995; Twardowski and Tonizzo 2018). Furthermore, light-scattering properties depend on the physical and chemical nature of water and its constituents and thus can provide biogeochemically useful information about water composition. For example, the particulate backscattering ratio, b_{bp}/b_p , can provide information about bulk particulate

*Correspondence: dkoestne@ucsd.edu

This is an open access article under the terms of the Creative Commons Attribution License, which permits use, distribution and reproduction in any medium, provided the original work is properly cited.

composition such as dominance of organic or inorganic particles in seawater (Twardowski et al. 2001; Boss et al. 2004; Koestner et al. 2018). Inverse methods have also been applied to measurements of $\beta_p(\psi)$ for natural particle assemblages to estimate particulate compositional and size information (Zhang et al. 2013). The particulate scattering and backscattering coefficients have been examined as proxies for estimating the mass concentrations of suspended particulate matter (SPM) (Babin et al. 2003; Neukermans et al. 2016), particulate inorganic carbon (Balch et al. 1999, 2001), particulate organic carbon (POC) (Stramski et al. 1999, 2008), and chlorophyll *a* (Chl *a*) (Huot et al. 2008; Antoine et al. 2011; Barbieux et al. 2018) in ocean waters. The spectral slope of backscattering was used for estimating the characteristics of particle size distribution PSD from satellite or in situ measurements (Boss et al. 2001; Kostadinov et al. 2009; Slade and Boss 2015). However, the complexity and variability of natural particulate assemblages impose significant challenges for an understanding of bulk light-scattering properties of seawater in terms of detailed particle size and compositional characteristics (Babin et al. 2003; Stramski et al. 2004). This complexity is, for example, reflected in significant variations in the relationships between light-scattering properties and measures of phytoplankton and particle concentrations (Huot et al. 2008; Woźniak et al. 2010; Neukermans et al. 2012) and the lack of robust relationship between the spectral slope of b_b and particle size across different water types (Reynolds et al. 2016).

To realize the full potential of applications associated with light scattering in the ocean, further improvements are required in the fundamental understanding of the effects of particle size and compositional characteristics on variability in scattering across various marine environments. It has recently been demonstrated that classifying samples in terms of the ratio of POC/SPM, which serves as a bulk compositional proxy for the relative organic and inorganic contributions to particulate matter, has the potential to provide improved estimates of particle characteristics from optical measurements including light scattering (Woźniak et al. 2010; Reynolds et al. 2016). This approach deserves further investigation. Further studies of the role of the PSD in light scattering associated with diverse particle assemblages encountered across different marine environments are also needed.

The size of optically significant marine particles varies from submicron range to at least several hundreds of micrometers (Jonasz and Fournier 2007; Davies et al. 2014), thus the PSD is a major driver of variability in particulate scattering in the ocean. For example, theoretical modeling of idealized assemblages of homogenous spherical particles obeying a Junge-type power-law of PSD predicts that very small particles in the picoplankton and colloidal size range, i.e., less than about 2 μm in diameter, can be a dominant source of b_{bp} under typical open ocean conditions in the absence of phytoplankton bloom or significant presence of coccolithophores (Stramski and Kiefer 1991). The idealized

assumptions about marine particles imply that such theoretical modeling must be interpreted with caution, especially in terms of quantitative predictions for natural particle assemblages, as various scenarios of the scattering dominance by different particle-size fractions or types can be encountered in various environments (Stramski et al. 2004). Theoretical computations have also shown that nonhomogenous particles, for example, layered spheres, produce enhanced backscattering compared with homogenous spheres (Meyer 1979). This suggests that marine particles $> 1 \mu\text{m}$ in size, especially phytoplankton cells, can play a greater role in b_{bp} within the surface ocean waters than predicted from the assumption of homogenous spherical particles (Kitchen and Zaneveld 1992; Whitmire et al. 2010). Only a few studies have used an experimental approach based on particle-size fractionation of natural seawater samples to address the role of particle size in backscattering. One such study in the equatorial Pacific Ocean suggested that particles $< 3 \mu\text{m}$ in size contribute significantly to b_{bp} , accounting for over 50% of the bulk signal in most samples (Dall'Olmo et al. 2009). Twelve samples from mainly oligotrophic waters (Chl *a* $< 0.25 \text{ mg m}^{-3}$) with low particle concentration were analyzed using a flow-through system with and without a 3 μm cartridge filter. In another study, Organelli et al. (2018) also used a flow-through system to collect and filter seawater for measurements of PSD and b_{bp} for 22 samples collected along an Atlantic meridional transect. Compared to Dall'Olmo et al. (2009), a broader range of oceanic conditions was included and Organelli et al. (2018) concluded that particles $< 1 \mu\text{m}$ accounted for about 30–55% of b_{bp} . In both studies, light scattering was measured only at one scattering angle and no significant assessment of the observed variability in light scattering as it relates to particulate characteristics such as size distribution and composition was made. In addition, these studies performed limited investigation into how the reported size-based b_{bp} budgets may have been affected by imperfect fractionation.

To improve our understanding of the effects of particle size and composition on the light-scattering properties of seawater, we conducted laboratory measurements of $\beta_p(\psi)$ combined with comprehensive characterization of the particulate assemblages of natural seawater samples before and after particle-size fractionation. The experiments were made for eight seawater samples collected near San Diego, California, which represent significant variability in terms of concentration of suspended particles, PSD, and composition as assessed by the contributions of organic vs. inorganic and phytoplankton vs. nonalgal particulate components. Unlike previous light-scattering studies involving size-fractionation (Dall'Olmo et al. 2009; Organelli et al. 2018), we investigate the roles of particle size and composition for a broad angular range of light scattering from $< 1^\circ$ to 150° using a comprehensive suite of parameters for particle characterization in parallel with angle-resolved scattering measurements. The fractionation of samples was made with mesh filters of 5 and 20 μm pore sizes, which allows for the investigation of the fraction of particles which are small-sized and large-sized. To our knowledge, the role of large-sized particles ($> 20 \mu\text{m}$) has not been

evaluated experimentally in the past. Our study also includes the assessment of the effects on our results associated with unavoidable limitations of particle fractionation methodology.

Methods

Water samples

Seawater samples were collected in the region of San Diego, California, from June 2016 through March 2017. Two samples were collected at offshore locations aboard the R/V *Sprout* in mid-September. One sample was collected ~ 8 km offshore with Niskin bottles at a depth of ~ 20 m coinciding with the measurement of maximum chlorophyll *a* fluorescence. The other sample was collected ~ 2 km offshore at a near-surface depth using the ship's surface seawater intake. Four nearshore samples were collected at the Scripps Institution of Oceanography (SIO) Pier, three of which were collected during periods of relatively high phytoplankton abundance in summer 2016 and one collected after a significant rain event in March 2017. Two estuarine samples were collected 2 km inland in the San Diego River Estuary at different stages of high tide. The nearshore and estuarine samples were collected at a depth of about 1 m using either a bucket or a 5-liter Niskin bottle. Table 1 provides additional description of samples with their corresponding ID used throughout the article.

Approximately 30–40 L of seawater were collected from a single location for each experiment with onshore laboratory analysis completed within 8 h after sampling except for offshore samples which were completed within 24 h after sampling. Before analysis, water was stored in 20-liter carboys and protected from light. The water in carboys was homogenized by gentle mixing immediately prior to removing samples for subsequent analysis. Special care was taken to ensure that subsamples of seawater used for different measurements and analyses were treated similarly and collected from carboys within

Table 1. General sample information for the eight experiments including identifier used throughout the article (ID), location of sampling, date of sampling, and some key characteristics used as a general descriptor. The pier samples were collected at the Scripps Institution of Oceanography (SIO) Pier, the estuary samples were collected in the San Diego River Estuary, and offshore samples were collected at various locations offshore of San Diego.

ID	Location	Date	Key characteristics
P _N	Pier	30 Jun 2016	Nanophytoplankton abundant
P _M	Pier	12 Jul 2016	Mixed assemblage
P _D	Pier	26 Jul 2016	Microphytoplankton abundant
P _R	Pier	01 Mar 2017	After heavy rain
E _L	Estuary	09 Aug 2016	Lower high tide
E _H	Estuary	18 Aug 2016	Higher high tide
O _S	Offshore	15 Sep 2016	Surface water
O _C	Offshore	19 Sep 2016	Subsurface Chl <i>a</i> maximum

1 h of each other. All measurements were typically completed within a 4-h period.

Particle fractionation

Seawater for each sample was fractionated using high-precision woven nylon or polyester mesh filters with pore sizes of 5 and 20 μm (Spectrum Labs). A 20 × 20 cm square of mesh filter was placed in a customized plastic Buchner funnel with a 15-cm diameter opening for each filtration. Mesh filters were sonicated in a 2% acid detergent solution (Citranox) for at least 10 min followed by back-flushing with at least 5 L of 0.2 μm-filtered deionized water before each use. After each use, mesh filters were back-flushed with at least 5 L of 0.2 μm-filtered deionized water followed by soaking in 2% Citranox solution overnight.

Both the 5 and 20 μm mesh filters did not require any excess pressure beyond the gravitational force of the water head. The 5 μm mesh filter exhibited mild resistance to flow and seawater was trickled into the Buchner funnel at a rate of ~ 4 mL s⁻¹ to limit the overall pressure exerted on suspended particles being retained by the filter. The 20 μm mesh did not produce any noticeable resistance to flow and seawater was poured manually in a swirling pattern.

We acknowledge that the fractionation procedure cannot produce sharp cutoffs at the mesh sizes and we thus choose to refer to particles retained on the 20 μm mesh as “large,” particles collected in the 5 μm filtrate as “small,” and those collected in the 20 μm filtrate but retained on the 5 μm mesh as “medium.” To provide a quantitative metric of filtration efficiency, we use a nominal filter rating in percent following Sparks and Chase (2015):

$$F_r^{\text{MD}} = \left(1 - \frac{\text{emergent \# particles } D > \text{MD}}{\text{incident \# particles } D > \text{MD}} \right) \times 100\% \quad (1)$$

where D (μm) is an equivalent spherical diameter of the center of a size bin used in measurements with the Coulter technique (see below for more details), MD is the diameter of a sphere corresponding to the pore size of the mesh (i.e., 5 or 20 μm in our experiments), incident # particles refers to concentration of particles in the original sample before filtration (i.e., unfiltered sample), and emergent # particles refers to concentration of particles in the filtrate. In an ideal case of perfect fractionation, the numerator in Eq. 1 would be zero and hence F_r^{MD} would be 100%.

Particulate mass concentration and composition

The mass concentrations of SPM, POC, and Chl *a* were determined following filtration of each original seawater sample onto 25 mm Whatman glass fiber filters (GF/F) at low (≤ 120 mm Hg) vacuum. Ratios of these mass concentrations additionally serve as proxies of bulk compositional characteristics of the particulate assemblage. Filtration volumes ranged from 200 to 1400 mL depending on particle concentration.

The determinations of SPM were made with a standard gravimetric method (van der Linde 1998). We used prerinced (~ 500 mL 0.2 μm -filtered deionized water), precombusted (5 h at 450°C), and preweighed GF/F filters. Filters with retained particles were gently rinsed with 0.2 μm -filtered deionized water to remove residual salt and then dehydrated in a 60°C convection oven for at least 1 h before weighting with a high-precision (1 μg) microbalance (MT5, Mettler-Toledo). Filters were then stored in a desiccator and weighed two more times immediately following additional dehydration in oven. The values of SPM (g m^{-3}) were determined by subtraction of the blank filter mass and dividing by the volume of filtered seawater.

POC samples were filtered onto precombusted GF/F filters and organic carbon content was determined using a standard high temperature combustion method (Parsons et al. 1984). Filters with retained particles were dehydrated and stored in acid-washed glass scintillation vials before analysis. Following acidification with 150 μL 10% HCl to remove inorganic carbon, the organic carbon mass of each filter was determined with a CEC 440HA Elemental CHN Analyzer (Control Equipment, now Exeter Analytical). The values of POC (mg m^{-3}) were determined by subtracting the average carbon mass of several blank filters and dividing by the volume of filtered seawater.

Chl *a* was measured using a spectrophotometric method. GF/F filters with retained particles were extracted overnight in 90% acetone, centrifuged, and the absorbance of the clarified acetone extract determined in a dual-beam spectrophotometer (Lambda 18, Perkin-Elmer) equipped with a 15-cm integrating sphere (RSA-PE-18, Labsphere). Following subtraction of the blank (90% acetone solution), values of Chl *a* in the acetone extracts were calculated using the four-band equation of Ritchie (2008) and scaled by filtration volume to obtain the final Chl *a* (mg m^{-3}) in the seawater sample.

For both the SPM and POC measurements, duplicate sample filters were collected and the results averaged to obtain the final estimates of SPM and POC for a given unfiltered seawater sample. Single filters were also collected to determine both SPM and POC for the 5 μm -filtrate of all seawater samples with the exception of one sample (P_N). Determination of Chl *a* for the unfiltered sample was performed using single filters and no determinations were made for the filtrates.

Particle size distribution

The measurements of PSD were made using an electronic impedance method with a Multisizer 3 (Beckman Coulter) equipped with a 100 μm aperture which allows particle counting in the size range of volume-equivalent spherical diameters, *D*, from 2 to 60 μm . Within this range, 300 logarithmically spaced size bins were used to produce high-resolution PSDs. A baseline measurement of 0.22 μm -filtered seawater was subtracted from sample measurements. Approximately 10–15 replicate measurements of 2 mL subsamples of each original

(unfiltered) and two size-fractionated samples (i.e., the 5 and 20 μm filtrates) were collected. Care was taken to ensure particles were well mixed and remained in suspension by manual stirring between replicate measurements. After removing outlier measurements, the remaining measurements were summed and divided by the total volume evaluated to produce an average PSD in particle counts per bin per unit volume of seawater.

We report various metrics of the PSD and provide graphical representation of the density function of particle number distribution, $N(D)$ ($\text{cm}^{-3} \mu\text{m}^{-1}$), which results from the normalization of particle number concentration in each size bin by the width of each bin. Assuming spherical shape of particles, the particle-volume distributions, $V(D)$, were determined from the number distributions for each sample. From $V(D)$, the percentile-based particle diameters were calculated such as the median diameter, D_v^{50} , and the 90th percentile diameter, D_v^{90} . These parameters have been shown to provide potentially useful metrics in the analysis of relationships between the optical and particle size properties in seawater (Woźniak et al. 2010).

Light scattering by particles

Measurements of the particulate volume scattering function, $\beta_p(\psi)$ ($\text{m}^{-1} \text{sr}^{-1}$), were made with the LISST-VSF instrument (Sequoia Scientific) in a laboratory benchtop configuration. For each sample, $\beta_p(\psi)$ was measured on the original (unfiltered) sample and two size-fractionated samples. The LISST-VSF measures angular scattering at light wavelength of 532 nm with an incident laser beam of ~ 3.2 mm in diameter. The intensity of light scattered was measured at angles ψ between 0.09° and 15.17° with 32 ring detectors and between 14° and 155° with 1° resolution using a roving eyeball sensor (photomultiplier tube). The geometry of measurement with the roving eyeball sensor results in interrogated sample volumes in the range ~ 0.1–0.3 mL depending on the scattering angle. The interrogated volume for the ring detectors is somewhat larger because the scattering contributions to these detectors are generated along a more significant portion of the 15 cm pathlength of the instrument. Beam attenuation was also measured over a 15 cm pathlength to provide an estimate of the particulate beam attenuation coefficient, c_p (m^{-1}), and to correct light scattering measurements for attenuation losses along the interrogated path of the sample. The volume of water necessary for benchtop use of our LISST-VSF is ~ 1.8 L and each measurement takes ~ 4 s. Extra care was taken to thoroughly clean the benchtop chamber before measurements of each unfiltered and size-fractionated sample by flushing with 0.2 μm -filtered deionized water. A thorough analysis of this specific instrument and measurement configuration has been previously performed, including formulation of a calibration correction and validation of $\beta_p(\psi)$ measurements (Koestner et al. 2018). Therefore, the description below emphasizes only some methodological aspects of LISST-VSF measurements conducted in this study.

All reported data of $\beta_p(\psi)$ represent the particulate scattering with molecular water scattering and scattering from very

small particles (less than about 0.2 μm) removed from the sample measurement via subtraction of a baseline measurement on filtered seawater. Approximately 2 L of 0.22 μm -filtered seawater were prepared via two filtrations at low vacuum; first, with a 47 mm diameter GF/F filter and then with a 47 mm diameter 0.22 μm nitrocellulose membrane filter. The 0.22 μm -filtered seawater was recirculated in the LISST-VSF chamber with a peristaltic pump and 0.2 μm Polycap 36 TC cartridge filter (Whatman) for at least 45 min to obtain the least contaminated baseline measurement. The particle concentration of the samples was adequate to ensure that measurements satisfy the single-scattering condition (van de Hulst 1981; Koestner et al. 2018). One sample (E_L) was diluted to reduce c_p to a value $< 2 \text{ m}^{-1}$ in order to satisfy this condition. Reported results for E_L account for this dilution.

Between four and eight sequences of 50 replicate measurements were collected for each unfiltered and size-fractionated sample with gentle hand mixing between sequences while a 5 cm magnetic stir bar was rotating at very low speed changing direction every 30 s. Thus, the final results of $\beta_p(\psi)$ are based on 200–400 replicate measurements depending on the sample. As a result, the total volumes interrogated with the eyeball sensor in the analysis of our samples varied between ~20 and 120 mL depending on the eyeball scattering angle, and were somewhat larger for the ring detectors. The determinations of final $\beta_p(\psi)$ involved quality control of replicate measurements, removing outliers potentially affected by measurement artifacts, and then deriving the median value at each angle from the remaining measurements.

To estimate the b_p and b_{bp} from the measured $\beta_p(\psi)$, an extrapolation procedure has been used to provide data within the angular range 151–180° as described in Koestner et al. (2018). In brief, a factor κ was determined to estimate the contribution of scattering within the range 151–180° to b_{bp} by finding the best fit function to our measured $\beta_p(\psi)$ between 90° and 150° and then extrapolating the fit function to 180°. Having determined b_p and b_{bp} , the backscattering ratio was calculated as $\tilde{b}_{bp} = b_{bp}/b_p$.

Light absorption by particles

For the measurement of spectral absorption coefficient of particles, $a_p(\lambda)$ (m^{-1}), unfiltered seawater samples were filtered onto 25 mm GF/F filters at low vacuum. Filtration volumes ranged from 100 to 800 mL depending on particle concentration in the samples. The $a_p(\lambda)$ coefficient was determined in the spectral range from 300 to 850 nm at 1 nm intervals using a Lambda 18 UV/VIS spectrophotometer (Perkin Elmer) equipped with a 15 cm integrating sphere (RSA-PE-18, Labsphere). In these measurements, we used a special “inside-sphere” configuration of the filter-pad technique with a sample filter placed inside the integrating sphere, which efficiently minimizes the scattering error (Röttgers and Gehnke 2012; Stramski et al. 2015). Duplicate spectral scans were made and averaged for two

orientations of the filter to account for any spatial inhomogeneity of particulate matter retained on the filter. An average baseline obtained from measurements of several blank filters saturated with 0.22 μm -filtered seawater was subtracted from the measurements of sample filters. The calculation of $a_p(\lambda)$ involved the use of the pathlength amplification correction recommended by Stramski et al. (2015).

Following the measurement of $a_p(\lambda)$, the sample filters were immediately subject to treatment with 95% methanol, which aims at removing the absorption contribution by extractable phytoplankton pigments (Kishino et al. 1985). The methanol-treated filters were then measured with the same inside-sphere spectrophotometric configuration. The result of this measurement is typically referred to as the spectral absorption coefficient of nonalgal particles or detrital particles, which is often denoted by $a_d(\lambda)$. The final $a_p(\lambda)$ and $a_d(\lambda)$ spectra were obtained by smoothing the respective spectral curves with a 5 nm moving average and correcting the $a_d(\lambda)$ spectra with an offset which ensured that the $a_d(\lambda)$ values match the $a_p(\lambda)$ values in the near-infrared spectral region (775–800 nm). As a final step of absorption data processing, the spectral absorption coefficient of phytoplankton was calculated as $a_{ph}(\lambda) = a_p(\lambda) - a_d(\lambda)$.

Light scattering budget based on particle-size fractionation

The measurements of $\beta_p(\psi)$ on unfiltered and size-fractionated samples allow the calculation of a light scattering budget based on particle size. Specifically, we define the scattering budget for $\beta_p(\psi)$ associated with small, medium, and large particle-size fractions as follows:

$$\begin{aligned}\beta_{ps}(\psi) &= \beta_p(\psi)[5 \mu\text{m filtrate}], \\ \beta_{pm}(\psi) &= \beta_p(\psi)[20 \mu\text{m filtrate}] - \beta_p(\psi)[5 \mu\text{m filtrate}], \\ \beta_{pl}(\psi) &= \beta_p(\psi)[\text{unfiltered}] - \beta_p(\psi)[20 \mu\text{m filtrate}],\end{aligned}\quad (2)$$

where subscripts s, m, and l stand for small, medium, and large particle-size fractions, respectively, and [5 μm filtrate], [20 μm filtrate], and [unfiltered] refer to the type of sample used in the measurement of $\beta_p(\psi)$. Note that the lower particle size limit in our measurements is about 0.2 μm because the baseline measurement was made with the 0.22 μm -filtered seawater. We also applied the same scheme and notation of scattering budget for b_p and b_{bp} . The percent contributions by each particle-size fraction to total particulate scattering by unfiltered samples were also computed for $\beta_p(\psi)$, b_p , and b_{bp} . For example, the percent contribution of the small particle-size fraction to total b_{bp} of unfiltered sample is $100 \times (b_{bps}/b_{bp})$.

Adjustment for imperfect particle-size fractionation

An analysis to investigate the effect of imperfect fractionation on the results for b_p and b_{bp} budgets was performed using theoretical light scattering computations for measured and idealized PSDs. We made these calculations using a particle scattering model of Xu et al. (2017) under the assumption that scattering calculations for hexagonally shaped particles

can reproduce angular light scattering by natural assemblages of marine particles more adequately than calculations for spherical particles. Adjustment factors describing the fractional difference in theoretical light scattering for idealized fractionation relative to theoretical scattering for actual fractionation were determined as follows:

$$\xi_x = \frac{b_{px}^I}{b_{px}^M} \quad (3)$$

$$\xi_{bx} = \frac{b_{bpx}^I}{b_{bpx}^M} \quad (4)$$

where subscript x is the particle-size fraction (s, m, or l), ξ_x and ξ_{bx} are the adjustment factors for b_{px} and b_{bpx} , respectively, and superscript I or M denotes whether the ideal or measured PSD was used as input for the scattering calculations. By ideal, we mean the PSD corresponding to a hypothetical perfect size-fractionation with fractionation efficiency F_r^{MID} of 100% (see Eq. 1) and without any effect on particles smaller than the pore size of the mesh filter. Accordingly, the ideal PSD of 5 μm filtrate is equivalent to the measured PSD of unfiltered sample for all size bins associated with particles smaller than 5 μm in diameter and has null particle concentration for all size bins larger than 5 μm . Similarly, the ideal PSD of 20 μm filtrate is equivalent to the measured PSD of unfiltered sample for all size bins associated with particles smaller than 20 μm in diameter and has null particle concentration for all size bins larger than 20 μm .

Because the particle size measurements covered the range 2–60 μm , for the purpose of this analysis, we extrapolated the measured PSDs down to 0.2 μm and up to 200 μm which improves the representation of optically significant size range. Extrapolations were performed by determining a slope parameter of power function fit to the measured PSD. The extrapolation from 2 to 0.2 μm used a slope parameter determined from size bins between 2.1 and 3.5 μm and extrapolation from 60 to 200 μm used a slope parameter determined from bins between 20 and 55 μm . Note that the idealized PSDs for 5 and 20 μm filtrates do not require an independent extrapolation to 0.2 μm because below 5 and 20 μm , these PSDs are identical to the measured PSDs of unfiltered samples including their extrapolated portions to 0.2 μm .

To compute theoretical scattering and backscattering coefficients for our extrapolated measured and idealized PSDs, we first calculated $\beta_p(\psi)$ for each PSD. Using an idealized PSD for an example,

$$\beta_p^I(\psi, n) = \sum_{D=0.2\mu\text{m}}^{D=200\mu\text{m}} N^I(D) \Delta D \sigma_b(\psi, n, D), \quad (5)$$

where D is an equivalent spherical diameter of the center of a given size bin (m), ΔD is the width of the bin (m), $N^I(D) \Delta D$ is

the particle number concentration (m^{-3}) in the bin as obtained from idealized PSD, n is the assumed complex refractive index of particles relative to water, and σ_b is the differential scattering cross section ($\text{m}^2 \text{sr}^{-1}$) calculated from the particle scattering model (Xu et al. 2017). We integrated the theoretical $\beta_p(\psi)$ within the angular range from 0.09° to 150° of LISST-VSF instrument and used the κ determined from the measured $\beta_p(\psi)$ (as described above) to derive theoretical values of b_p and b_{bp} . Following Eq. 2, we then determined the necessary inputs for Eqs. 3, 4 and subsequently the corresponding ξ_x and ξ_{bx} .

For each sample, these calculations were repeated for five values of the real part of refractive index, which were chosen to reasonably cover a range of the bulk refractive index for natural assemblages of marine particles (Zaneveld et al. 1974; Jonasz and Fournier 2007). For samples dominated by organic particles with the largest contribution of phytoplankton (P_N , P_N , P_D , and O_C as described below in the “Results” section), we used the refractive index relative to water from 1.03 to 1.07 with a 0.01 step (Aas 1996; Stramski et al. 2001). For samples dominated by inorganic particles with the lowest contribution of phytoplankton (E_L and E_H), we used the values from 1.09 to 1.13 with a step of 0.01 (Carder et al. 1974; Woźniak and Stramski 2004). For the two remaining samples with intermediate contribution of phytoplankton (P_R and O_S), we used the values from 1.06 to 1.10 with a step of 0.01. In all these calculations, we used one value of the imaginary part of refractive index of 0.0005, which reasonably represents weak absorption at 532 nm.

For each sample, the final adjustment factors ξ_x and ξ_{bx} were determined for each particle-size fraction as the average of the adjustment factors determined from calculations made for all five values of the refractive index. The final ξ_x and ξ_{bx} were multiplied by our LISST-VSF measured b_{px} and b_{bpx} to yield a final result of our analysis which provides an assessment of the potential effect associated with imperfect fractionation. Using small particle-size fraction as an example,

$$b_{ps}^* = b_{ps} \xi_s, \quad (6)$$

$$b_{bps}^* = b_{bps} \xi_{bs}, \quad (7)$$

where * indicates that the measured scattering and backscattering coefficients have been adjusted for imperfect fractionation. Compared to the actual size-fractionated measurements, the adjusted coefficients b_{ps}^* and b_{bps}^* refer more rigorously to particles smaller than 5 μm in diameter, b_{pl}^* and b_{bpl}^* refer to particles larger than 20 μm , and b_{pm}^* and b_{bpm}^* refer to particles in the 5–20 μm range.

Finally, using the scattering and backscattering coefficients adjusted for imperfect fractionation, the adjusted percent contributions of each particle-size fraction to total b_p and b_{bp} of unfiltered samples were computed. For example, the adjusted

percent contribution of small particle-size fraction, which in this case corresponds more rigorously to particles $< 5 \mu\text{m}$ in size, to total b_{bp} of unfiltered sample is $100 \times (b_{\text{bps}}^*/b_{\text{bp}})$.

Results

Assessment of particle-size fractionation

Filtration efficiency for natural assemblages of aquatic particles is complex and depends on many factors, including filter type, loading rate, and particle composition and shape (Sparks and Chase 2015). As a means of assessing the particle-size fractionation through filtration with the 5- and 20- μm mesh filters, we compared measurements of PSD on the unfiltered samples with size-fractionated samples. Figure 1 shows an example of such measurements for the E_{H} sample. In general, there is adequate retention by the mesh of particles larger than the pore size of the mesh. However, fractionation is nonideal in the sense that some particles smaller than the pore size are retained on the mesh and some particles larger than the pore size are found in the filtrate. For example, in Fig. 1, we see that retention of particles by the 20 μm mesh starts to increase significantly around 10 μm and particles larger than 20 μm are still present in the filtrate (solid green line), albeit at much lower concentrations compared with the unfiltered sample (solid red line). Under the condition of ideal fractionation, the PSD of the 20 μm filtrate would be identical

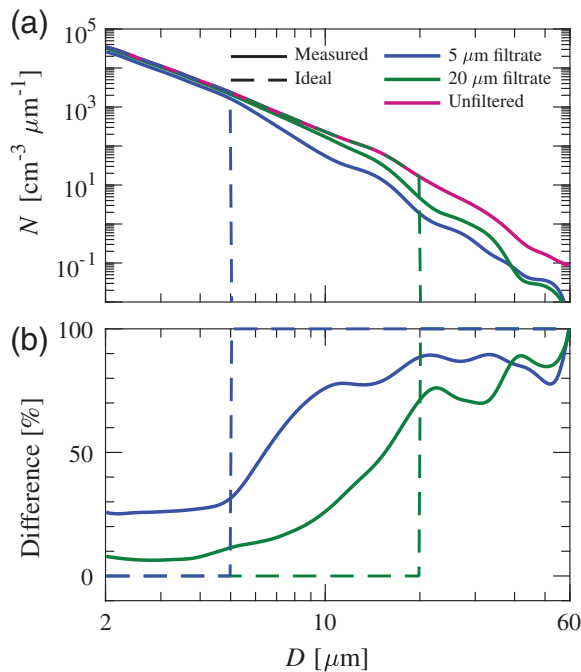


Fig. 1. (a) Particle size distributions as density functions of particle number concentration, N , for unfiltered and size-fractionated samples from the San Diego River Estuary (sample E_{H}). (b) Percent difference between the size-fractionated samples and the unfiltered sample shown in (a). Solid lines represent the measured size distribution and dashed lines represent idealized size-fractionation.

Table 2. Filter ratings, F_r^{MD} where MD is the pore size of filter mesh in μm , and the volume-equivalent spherical diameter D associated with $F_r = 80\%$ for the 5 and 20 μm mesh filters. F_r^{MD} was calculated using Eq. 1 and PSD data from each experiment.

ID	5 μm mesh		20 μm mesh	
	F_r^5 (%)	D ($F_r = 80\%$) (μm)	F_r^{20} (%)	D ($F_r = 80\%$) (μm)
P_{N}	24	16.0	10	28.6
P_{M}	21	14.0	24	28.9
P_{D}	21	14.8	15	49.2
P_{R}	60	8.02	74	28.2
E_{L}	42	8.58	36	47.0
E_{H}	56	10.2	75	31.6
O_{S}	30	33.8	-29	41.0
O_{C}	28	19.0	45	33.5

to that for the unfiltered sample in the range $D < 20 \mu\text{m}$ and the particle concentration would drop to zero at 20 μm and beyond (dashed green line). Similarly, Fig. 1 shows that the 5 μm filtrate contains particles larger than 5 μm although at significantly lower concentrations compared with the unfiltered sample. While the filtration efficiency may be affected by several factors, it is also critical to recognize that our PSDs are determined for volume-equivalent spherical diameters, so the unknown degree of nonsphericity of particles suspended in the samples can influence the fractionation results.

Filter ratings for the 5- and 20- μm mesh filters calculated following Eq. 1 are shown in Table 2 for all eight samples examined in this study. We also display the particle diameter associated with $F_r = 80\%$ as an additional metric for assessing filtration efficiency. This value denotes the threshold diameter at which 80% of the total counts of particles larger than this threshold have been retained on the mesh and hence removed from the liquid phase of the sample during fractionation. Although this 80% threshold is chosen somewhat arbitrarily, it provides a measure of particle diameter at which substantial fractionation is achieved.

Data in Table 2 show significant retention of particles $> 5 \mu\text{m}$ by the 5 μm mesh with F_r^5 ranging from 21% to 60%. The threshold diameter associated with 80% retention is $< 16 \mu\text{m}$ with the exception of two offshore samples. The 20 μm mesh shows a larger range of filter rating compared with that for the 5 μm mesh. The threshold diameter associated with 80% retention of particles by the 20 μm mesh is typically about 30 μm with the exception of three samples with values exceeding 40 μm . The evaluation of the 20 μm mesh is complicated by the fact that particles with $D > 20 \mu\text{m}$ occur typically at very low concentrations in the samples ($< 10 \text{ particles cm}^{-3} \mu\text{m}^{-1}$), so the particle counting statistics obtained with the Coulter technique are typically limited for these relatively large diameters. In addition, particles with $D > 60 \mu\text{m}$ were beyond the size range of our PSD measurements. We also note one peculiar case (O_{S}) which has a negative F_r^{20} value indicating more particles with $D > 20 \mu\text{m}$ in the 20 μm

filtrate than in the unfiltered sample. This may result from low particle counts, possible disruption of larger particle aggregates, or both. Nonetheless, the diameter associated with 80% retention is $41\ \mu\text{m}$ in this case.

Not surprisingly, the results from this analysis support the notion that realistically achievable efficiencies of particle-size fractionation can differ considerably from an ideal fractionation scenario (Sheldon 1972; Logan 1993), even if seawater samples are subject to gentle filtration through high-precision mesh filters with relatively large pore size as was done in the present study. Nevertheless, we consider such fractionation a useful experimental approach for addressing the main objectives of our study because the fractionation produces a large change in the PSD, which is consistent with the pore size of the filter. However, because the pore size of the filter cannot be used in a quantitative sense as a strict cutoff size in the PSD, the particle-size fractions obtained from measurements on $5\ \mu\text{m}$ filtrates, $20\ \mu\text{m}$ filtrates, and unfiltered samples are qualitatively referred to as representing small, medium, and large particles as has been already explained in relation to Eq. 2.

Particle size and composition characteristics

The measured PSDs of the eight seawater samples are shown in Fig. 2. Each panel includes the additional PSD

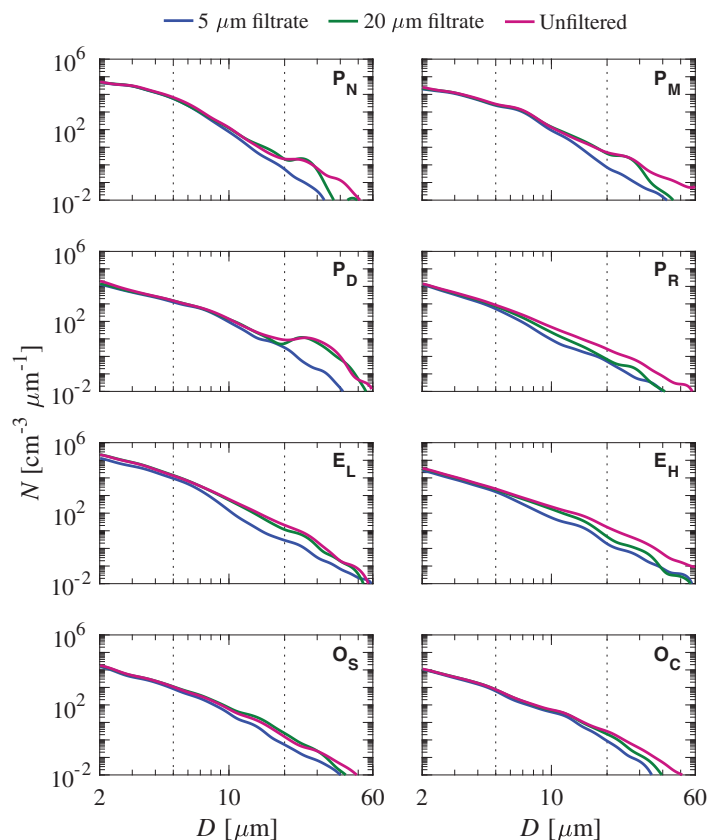


Fig. 2. Measured PSDs for unfiltered and size-fractionated samples for the eight seawater samples as indicated. Vertical black dotted lines are shown to represent the expected cutoff of the mesh filters at $5\ \mu\text{m}$ and $20\ \mu\text{m}$.

measurements for the two size-fractionated samples. The particle number concentrations span nearly seven orders of magnitude within the measured size range $2\text{--}60\ \mu\text{m}$ with the P_N and E_L samples exhibiting the highest concentrations approaching or surpassing $10^5\ \text{particles cm}^{-3}\ \mu\text{m}^{-1}$ at a diameter of $2\ \mu\text{m}$. None of the unfiltered samples (red lines in Fig. 2) appear to obey a Junge-type size distribution with a single slope of the log-log plot of PSD over the measured size range. In all cases, the slope exhibits significant changes as a function of particle diameter and in some cases, large features including maxima (e.g., P_N , P_M , and P_D) are superimposed on the general trend of decreasing particle concentration with increasing particle diameter. These results support earlier observations that the Junge-type distribution with a single slope often provides an inadequate approximation of PSD of marine particles (Jonasz and Fournier 2007; Reynolds et al. 2010; 2016). As expected, the deviations from a single slope distribution are much more pronounced for the size-fractionated samples, which can also exhibit significant features, especially in some $20\ \mu\text{m}$ filtrates.

Characterization of the PSDs using the percentile particle diameters, D_v^{50} and D_v^{90} , is provided in Table 3 for the unfiltered samples and the small particle-size fraction corresponding to the $5\ \mu\text{m}$ filtrates. The variations in D_v^{50} and D_v^{90} between the samples reflect varying contributions of small vs. large particles to the PSD. For example, the unfiltered samples P_D , P_R , and E_H have $D_v^{90} > 30\ \mu\text{m}$ indicating a significant contribution of large-sized particles while samples P_N , E_L , and O_S have D_v^{90} close to or less than $20\ \mu\text{m}$ indicating a greater role of small-sized particles. D_v^{50} is also useful in interpreting the PSD of unfiltered samples. For example, sample O_C has a lower D_v^{90} than sample P_M ; however, D_v^{50} is higher for O_C indicating that small-sized particles play less significant role in O_C compared to P_M . Among the eight examined samples of unfiltered seawater, sample P_N has the greatest role of small-sized particles (the lowest values of D_v^{50} and D_v^{90}) and sample P_D the greatest role of large-sized particles (the highest values of D_v^{50} and D_v^{90}). As expected, data for small-sized particles after fractionation with the $5\ \mu\text{m}$ mesh indicate a decrease in D_v^{50} and D_v^{90} compared with the corresponding unfiltered samples. For example, D_v^{50} is $< 7.5\ \mu\text{m}$ for the small-particle fraction of all samples. It is of interest to note that medium- or large-sized particles may still play a role in the small-particle fraction of some samples as suggested by relatively large values of D_v^{90} , especially $24.9\ \mu\text{m}$ for E_H and $18.1\ \mu\text{m}$ for P_D .

Table 3 also provides a comparison of samples in terms of particle mass concentration and composition characteristics. SPM, POC, and Chl *a* serve as metrics of bulk concentration of total particulate matter, organic particulate matter, and phytoplankton, respectively. The ratios POC/SPM, Chl *a*/SPM, and $a_{ph(440)}/a_p(440)$ are used as metrics of composition of particulate matter. Specifically, POC/SPM provides a proxy for

Table 3. Mass concentrations of SPM (g m^{-3}), POC (mg m^{-3}), and Chl *a* (mg m^{-3}) and particulate composition and size parameters derived from measurements on the unfiltered seawater samples from the eight experiments. Information is also displayed when available for the small particle-size fraction in the $5 \mu\text{m}$ filtrates. The absorption ratio is given at $\lambda = 440 \text{ nm}$. The particle size parameters, D_V^{50} and D_V^{90} , are the diameters in μm associated with the 50th and 90th percentile, respectively, of the particle volume distribution.

ID	Concentration			Composition			Size	
	SPM	POC	Chl <i>a</i>	POC/SPM	Chl <i>a</i> /SPM	$a_{\text{ph}}(440)/a_{\text{p}}(440)$	D_V^{50}	D_V^{90}
Unfiltered seawater								
P _N	1.13	532	2.49	0.47	0.0022	0.88	5.10	14.0
P _M	1.19	259	1.76	0.22	0.0015	0.77	7.41	28.6
P _D	0.75	453	2.26	0.60	0.0030	0.65	24.9	35.8
P _R	1.13	153	0.76	0.14	0.0007	0.50	8.78	30.2
E _L	9.90	873	3.00	0.09	0.0003	0.23	6.39	20.1
E _H	3.18	436	1.21	0.14	0.0004	0.25	13.5	34.6
O _S	0.54	192	0.53	0.35	0.0010	0.36	7.08	19.9
O _C	0.36	153	0.75	0.43	0.0021	0.71	9.84	25.8
Small particle fraction								
P _N	—	—	—	—	—	—	4.55	8.11
P _M	0.62	181	—	0.29	—	—	6.11	11.5
P _D	0.32	157	—	0.49	—	—	7.49	18.1
P _R	0.26	63	—	0.24	—	—	4.76	16.9
E _L	1.25	296	—	0.24	—	—	4.93	9.95
E _H	0.96	165	—	0.17	—	—	6.54	24.9
O _S	0.36	151	—	0.41	—	—	5.77	13.5
O _C	0.24	124	—	0.53	—	—	6.77	16.2

contributions of organic vs. inorganic particles to total mass of particulate matter. Both Chl *a*/SPM and $a_{\text{ph}}(440)/a_{\text{p}}(440)$ provide proxies for contributions of phytoplankton vs. nonalgal particles although the former in the context of particulate mass concentration and the latter in the context of particulate absorption. In Table 3, all these concentration and composition

parameters are listed for unfiltered samples and some parameters are also provided for the small particle-size fraction. The spectral information on the ratio $a_{\text{ph}}(\lambda)/a_{\text{p}}(\lambda)$ for unfiltered samples is also depicted in Fig. 3.

Among the eight original (unfiltered) samples examined, the offshore samples (O_S and O_C) have the lowest SPM ($\sim 0.5 \text{ g m}^{-3}$ or less) and the samples collected in the San Diego River Estuary (E_L and E_H) have the highest SPM in the range from about 3 to 10 g m^{-3} . The samples from the SIO Pier have intermediate values of SPM. The offshore samples also have the lowest POC and Chl *a*. The offshore values of Chl *a* ranged from about 0.5 to 0.75 mg m^{-3} , which is significantly higher than the average near-surface Chl *a* of about 0.2 mg m^{-3} within the global ocean (Gregg and Conkright 2002). Only one SIO Pier sample (P_R) has POC and Chl *a* that are comparable to the offshore values; the remaining samples are characterized by significantly higher values, including Chl *a* $> 2 \text{ mg m}^{-3}$ for P_N, P_D, and E_L. These data indicate that in terms of particle concentration, our samples are not representative of vast areas of oligotrophic open ocean where Chl *a* is $< 0.5 \text{ mg m}^{-3}$.

The composition of particulate assemblages also varies significantly among the unfiltered samples as characterized by the large range of POC/SPM from 0.09 to 0.6, i.e., from inorganic-dominated (E_L) to highly organic-dominated (P_D). The samples from San Diego River Estuary are inorganic-dominated with the lowest POC/SPM. Despite the relatively high Chl *a*, we presume

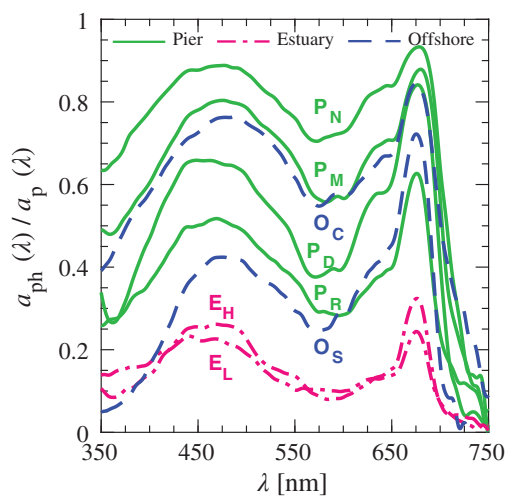


Fig. 3. The proportion of spectral particulate absorption coefficient associated with phytoplankton for the eight seawater samples as indicated.

phytoplankton to have minimal relative contribution to E_L and E_H as indicated by the lowest Chl a /SPM and $a_{ph}(440)/a_p(440)$ values (see also the spectra $a_{ph}(\lambda)/a_p(\lambda)$ in Fig. 3). Only one SIO Pier sample (P_R) has comparatively low POC/SPM of 0.14; the remaining samples have significantly higher values indicating a major or dominant role of organic particles.

Two SIO Pier samples (P_N and P_D) are totally dominated by organic matter with POC/SPM in the range 0.47–0.6. These samples also have relatively high values of Chl a /SPM and $a_{ph}(\lambda)/a_p(\lambda)$ indicating a dominant role of phytoplankton. We use some ancillary information (not shown) to help further characterize these samples. The P_N sample is most likely nanophytoplankton-dominated or perhaps even picophytoplankton-dominated. We note that the highest concentration of picoeukaryotes observed with flow cytometry measurements during summer 2016 (B. Palenik pers. comm.) corresponded to the period of collecting the P_N sample. Despite a conspicuous particle (most likely phytoplankton) population near 25 μm in the PSD of P_N (Fig. 2), half of the measured particle volume is associated with particles smaller than about 5 μm (Table 3) which, along with very high $a_{ph}(440)/a_p(440)$, supports the major role of small-sized phytoplankton cells in this sample. The P_D sample is considered to represent highly productive conditions related to the strong presence of microphytoplankton. This conjecture is supported by observations of an abundance of the chain-forming diatom *Hemiaulus hauckii* with the Scripps Plankton Camera System operated by the Jaffe Laboratory for Underwater Imaging during the time of collecting our P_D sample. This is also consistent with the PSD of P_D , which shows a large particle population centered around 30 μm . These diatom chains consist of individual cells of about 15 μm in base diameter by 100 μm in length, which produces a volume-equivalent spherical diameter of about 32 μm .

The offshore samples O_S and O_C are also highly organic-dominated with POC/SPM ranging from 0.35 to 0.43. However, as indicated by Chl a /SPM and $a_{ph}(\lambda)/a_p(\lambda)$, the role of phytoplankton in the particulate assemblage of surface sample O_S is significantly reduced compared to sample O_C that was collected within the subsurface Chl a maximum. We therefore presume O_S to be mostly organic and nonalgal in nature while O_C is phytoplankton-dominated.

Our analysis also includes one SIO Pier sample (P_M), which has an intermediate value of POC/SPM of 0.22. This value indicates a major role of organic particles with a non-negligible effect of inorganic particles. This particulate assemblage also has the second highest ratio of $a_{ph}(440)/a_p(440)$ of 0.77 (see also Fig. 3) suggesting a very important role of phytoplankton.

Table 3 also includes SPM, POC, and POC/SPM data for the small particle fractions corresponding to the 5 μm filtrates. Based on these data, the percent contribution of SPM associated with the small particle fraction to the total SPM associated with the unfiltered sample ranges between 13% and 67%. For POC, this range is 34–81%. For samples P_M , O_S , and O_C , over half of the total SPM and POC is associated with small particle fraction. With the exception of one sample (P_D), the ratio

POC/SPM is higher in the small particle fraction compared with unfiltered sample, indicating that the small particle fraction is usually more organic than the entire particulate assemblage. For example, the POC/SPM value for the small particle fraction of sample E_L increased almost threefold compared with the entire particulate assemblage (0.24 vs. 0.09), suggesting that while the entire assemblage is inorganic-dominated, the small particle fraction is organic-dominated and therefore the medium- and large-sized particles are even further dominated by inorganic particles (i.e., POC/SPM < 0.09). A similar trend is observed for sample P_R which exhibits an important role of inorganic particles in its unfiltered assemblage.

Particulate scattering properties

Figure 4 shows the particulate volume scattering functions, $\beta_p(\psi)$, and scattering phase functions, $\tilde{\beta}_p(\psi)$, measured on the eight unfiltered seawater samples. The San Diego River Estuary samples have the largest magnitude of $\beta_p(\psi)$ for nearly all scattering angles while offshore samples have the lowest values (Fig. 4a,b). Although the angular scattering patterns share the common features of a strong peak at forward angles and flattening in the backscattering region $\psi > 100^\circ$, which are characteristic for natural assemblages of aquatic particles (Morel 1973; Jonasz and Fournier 2007; Sullivan and Twardowski 2009), there are significant differences among our samples in the angular shape of scattering as shown by the scattering phase functions (Fig. 4c,d). In particular, the $\tilde{\beta}_p(\psi)$ functions

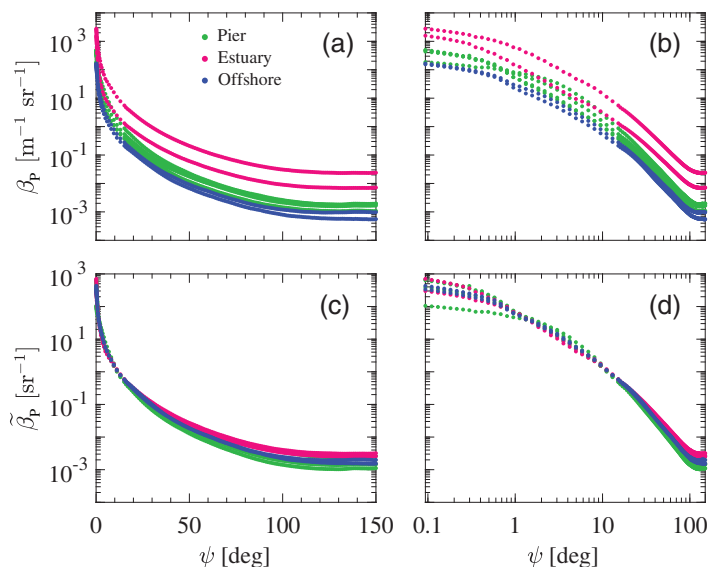


Fig. 4. (a, b) Measurements of the particulate volume scattering function, $\beta_p(\psi)$, and (c, d) the particulate scattering phase function, $\tilde{\beta}_p(\psi)$, at light wavelength of 532 nm for the unfiltered seawater samples as indicated. The left panels (a, c) depict $\beta_p(\psi)$ and $\tilde{\beta}_p(\psi)$ with linear scaling of scattering angles between 0° and 150° while the right panels (b, d) depict $\beta_p(\psi)$ and $\tilde{\beta}_p(\psi)$ with logarithmic scaling of angles between 0.1° and 150° . Data points represent median values.

Table 4. Particulate scattering, b_p , and backscattering, b_{bp} , coefficients at $\lambda = 532$ nm determined from measurements of $\beta_p(\psi)$ for unfiltered seawater samples from the eight experiments. Information is also displayed for the small particle-size fraction in the 5 μm filtrates. The values of the backscattering ratio, $\tilde{b}_{bp} = b_{bp}/b_p$, are also shown.

ID	Unfiltered seawater			Small particle fraction		
	b_p (m^{-1})	b_{bp} (m^{-1})	\tilde{b}_{bp}	b_p (m^{-1})	b_{bp} (m^{-1})	\tilde{b}_{bp}
P _N	1.75	0.0135	0.008	1.57	0.0109	0.007
P _M	1.13	0.0116	0.010	0.76	0.0074	0.010
P _D	0.73	0.0078	0.011	0.33	0.0039	0.012
P _R	0.75	0.0135	0.018	0.41	0.0058	0.014
E _L	9.25	0.1690	0.018	2.56	0.0493	0.019
E _H	2.23	0.0498	0.022	0.78	0.0181	0.023
O _S	0.49	0.0068	0.014	0.35	0.0049	0.014
O _C	0.36	0.0042	0.012	0.30	0.0033	0.011

of the estuary samples exhibit enhancements within the range encompassing intermediate and backscattering angles, $\psi > 45^\circ$. The SIO Pier samples generally have the lowest values of $\tilde{\beta}_p(\psi)$ in this range of scattering angles while the offshore samples have the intermediate values. Within the near-forward scattering region where ψ is less than about 10° , the angular shapes of $\tilde{\beta}_p(\psi)$ are generally similar between the samples, although the SIO Pier sample P_N stands out in this region with enhancement between about 2° and 8° and a flattening for $\psi < 1^\circ$, while data for all other samples continue to rise more substantially with further decrease in scattering angle (Fig. 4d).

Table 4 shows b_p and b_{bp} computed from the measured $\beta_p(\psi)$ as well as the backscattering ratio, \tilde{b}_{bp} , for the unfiltered samples and 5 μm filtrates (i.e., small particle fraction). The b_p and b_{bp} coefficients generally follow the trends observed in the magnitude of $\beta_p(\psi)$ as displayed in Fig. 4a,b, while \tilde{b}_{bp} generally reflects the variations in $\tilde{\beta}_p(\psi)$ shown in Fig. 4c,d. The estuary samples (E_L and E_H) have the highest values for both b_p and b_{bp} , which is consistent with the highest particle mass concentration of these samples (SPM in Table 3). The offshore samples (O_S and O_C) have the lowest values of b_p and b_{bp} , which is consistent with the lowest values of SPM for these samples. For the SIO Pier samples, b_p and b_{bp} assume intermediate values between the estuary and offshore samples. There are, however, notable differences between the pier samples. For example, whereas b_{bp} for P_N and P_R are nearly identical, b_p for P_N is over twice as large as it is for P_R. The P_D sample has the lowest values of b_p and b_{bp} among the pier samples, which is especially well pronounced for b_{bp} .

The backscattering ratio, \tilde{b}_{bp} , varies over a 2.75-fold range between 0.008 for P_N and 0.022 for E_H. This range is consistent with earlier observations of \tilde{b}_{bp} in different marine environments (Boss et al. 2004; Antoine et al. 2011). The most inorganic-dominated samples with the lowest POC/SPM ratio (P_R, E_L, and E_H) have the highest \tilde{b}_{bp} values, which suggest that these assemblages are dominated by particles having a relatively

high refractive index (Twardowski et al. 2001). The sample P_N with the lowest \tilde{b}_{bp} is highly organic and phytoplankton-dominated (Table 3). Interestingly, although P_N also has the lowest values of particle size metrics as shown in Table 3, this relative importance of small particles does not seem to have a clear enhancement effect on \tilde{b}_{bp} . We also recall that, in contrast to other samples, P_N exhibits enhancement in the phase function $\tilde{\beta}_p(\psi)$ between about 2° and 8° (Fig. 4d), which may contribute to lower \tilde{b}_{bp} by means of increased b_p .

Data in Table 4 also show that the \tilde{b}_{bp} values of the small particle-size fraction are generally very similar (to within ± 0.001) to the values of unfiltered samples. The only exception is the sample P_R for which \tilde{b}_{bp} of the small particle-size fraction decreased by 0.004 compared to the unfiltered sample. This sample is characterized by the noteworthy increase of POC/SPM in the small size fraction compared to the unfiltered sample (0.24 vs. 0.14, Table 3). Nevertheless, the interpretation of the potential effect of changes in particle composition on \tilde{b}_{bp} of sample P_R as a result of size fractionation is not straightforward because most other samples also showed an increased POC/SPM in the small size fraction (Table 3). In addition, \tilde{b}_{bp} is dependent on particle size which, on average, is smaller in the small particle-size fraction than the unfiltered sample (Table 3) and, hence, expected to enhance \tilde{b}_{bp} (Morel and Bricaud 1986).

With regard to data for the small particle-size fraction, Table 4 also shows an expected decrease in the magnitudes of b_p and b_{bp} compared with the unfiltered samples. This reduction is a component of the particle size-based scattering budget which is discussed in greater detail in the next section. In brief, the data for the eight examined samples displayed in Table 4 indicate a significant range in the extent to which b_p and b_{bp} are reduced in the small particle-size fraction compared to the unfiltered samples. For example, this reduction for backscattering is only about 20–30% for P_N, O_S, and O_C and as much as 65–70% for E_L and E_H. This result indicates

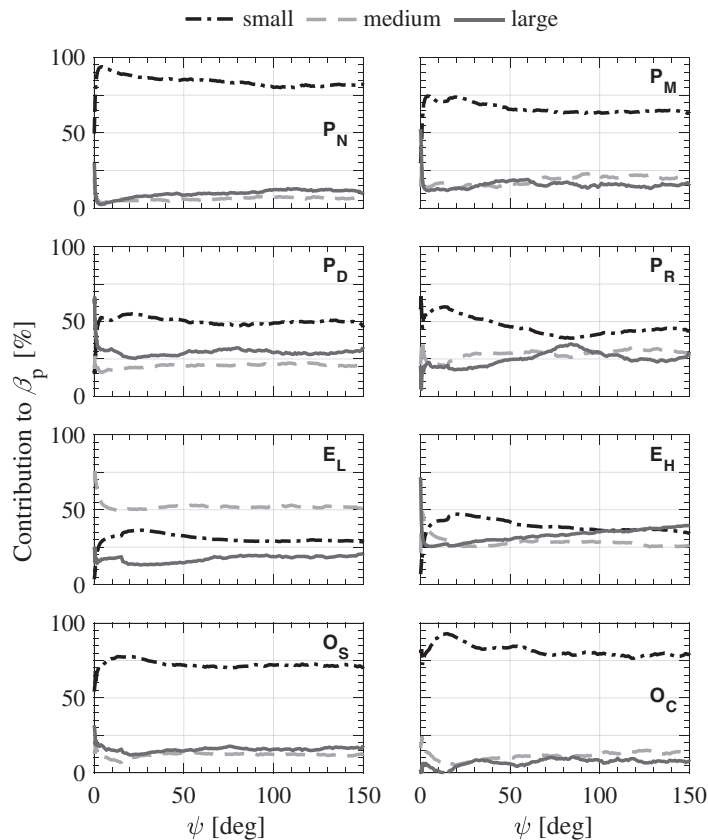


Fig. 5. Particulate scattering budget in terms of contributions of particle-size fractions to the total particulate volume scattering function, $\beta_p(\psi)$, in the range of scattering angles $0.09\text{--}150^\circ$ for the eight seawater samples as indicated. Results for small, medium, and large particle-size fractions are shown as a percentage of the total $\beta_p(\psi)$.

that our study includes a range of contrasting samples with highly different scenarios for particulate backscattering in terms of the roles of the small particle-size fraction.

Figure 5 shows the relative contributions of small [$\beta_{ps}(\psi)$], medium [$\beta_{pm}(\psi)$], and large [$\beta_{pl}(\psi)$] particle-size fractions to the total particulate volume scattering function, $\beta_p(\psi)$, for each experiment using the notation described in Eq. 2. Generally, the small particles dominate $\beta_p(\psi)$ at nearly all scattering angles for all samples except E_L and E_H . Samples P_N and O_C exhibit the highest contributions of $\beta_{ps}(\psi)$ to $\beta_p(\psi)$, generally greater than 75%, and samples P_M and O_S also have very high contributions generally in the range of 65–75%. For samples P_D and P_R , the contributions vary between about 40% and 55%. For sample E_L , the scattering by medium-sized particles, $\beta_{pm}(\psi)$, is the most important contributor to $\beta_p(\psi)$ while E_H exhibits a pattern with most similar contributions of all three particle-size fractions. We also note that, with the exception of E_L , the contributions of $\beta_{pm}(\psi)$ and $\beta_{pl}(\psi)$ to $\beta_p(\psi)$ are quite comparable to one another. Another interesting feature is a significant decrease in the contribution of $\beta_{ps}(\psi)$ to $\beta_p(\psi)$ at small scattering angles less than about 10° , which is consistent with the notion of general dominance of near-forward scattering by larger particles (Morel and Bricaud 1986; Jonasz and

Fourrier 2007). Otherwise, the scattering-budget curves in Fig. 5 are mostly flat as a function of ψ .

Discussion

This study is based on a suite of simultaneous measurements of light scattering and several metrics of particulate concentration, composition, and size distribution of contrasting natural seawater samples, including measurements on particle size-fractionated samples. Owing to this approach, our results provide unique insights into the complexity of the roles played by particle size and composition in light scattering produced by highly variable natural assemblages of aquatic particles. We examined eight contrasting samples from nearshore and coastal oceanic environments including river estuary and offshore samples. Samples P_N , P_D (from SIO Pier), and O_C (from subsurface Chl *a* maximum at offshore location) are all highly dominated by organic particulate matter, which includes strong contribution of phytoplankton as indicated by the highest values of POC/SPM accompanied by high values of Chl *a*/SPM and a_{ph}/a_p (Table 3). Despite sharing these common features, these three samples are highly contrasting because P_N exhibits the greatest relative role of small-sized particles (mainly nanophytoplankton and picophytoplankton cells) and P_D the greatest role of large-sized particles (mainly chain-forming diatoms) among all examined samples (Table 3). Samples E_L and E_H (from San Diego River Estuary) provide strong contrast with other samples because of predominance of inorganic particles and the smallest relative role of phytoplankton (Table 3). Again, despite sharing common features, E_L and E_H differ significantly from one another in terms of particle size characteristics with E_L having a higher proportion of small- vs. large-sized particles (Table 3). Samples P_M , P_R (SIO Pier), and O_S (surface water at offshore location) provide additional contrasting features (Table 3). Specifically, O_S is dominated by organic particles but it is the nonalgal component, rather than phytoplankton, which is most important. Sample P_R was collected after rain event and hence is characterized by dominant presence of inorganic particles although phytoplankton still make an important contribution to particulate absorption. Finally, sample P_M appears to represent an intermediate scenario of transition between inorganic- and organic-dominated particulate assemblage that includes, however, a major role of phytoplankton.

Our results obtained with such contrasting samples support long-recognized challenges for the use of particulate scattering and backscattering coefficients as empirical proxies for phytoplankton or particulate concentration metrics, such as Chl *a* (Huot et al. 2008; Antoine et al. 2011; Barbieux et al. 2018), POC (Stramski et al. 2008; Woźniak et al. 2010), and SPM (Babin et al. 2003; Neukermans et al. 2016). For example, samples P_N and P_R are characterized by nearly identical b_{bp} and SPM but differ greatly from one another in terms of b_p , POC and Chl *a*, as well as all particulate composition and size metrics determined in our

experiments (Tables 3–4). Another example is provided by a comparison of samples P_R and O_C , which are characterized by nearly identical Chl a and POC but very different b_p , b_{bp} , SPM, and particulate composition metrics.

In view of such complexities, our data obtained for the original (unfiltered) and size-fractionated samples provide particularly useful insights on the intricate effects of particle size and composition on light scattering. Specifically, measurements of angle-resolved scattering provided information on the contributions of three particle-size fractions, referred to as small, medium, and large size fractions, to total magnitude of particulate volume scattering function, $\beta_p(\psi)$, at different scattering angles ψ for each examined sample (Fig. 5). These measurements also allow the determination of similar particle size-based budgets for the particulate scattering, b_p , and backscattering, b_{bp} , coefficients. Because of specific needs to advance an understanding of the backscattering coefficient owing to its effect on ocean reflectance and ocean color remote sensing (Morel and Prieur 1977; Gordon

and Morel 1983) as well as increasing potential for applications associated with extensive use of backscattering sensors on autonomous in situ platforms (Organelli et al. 2017; Barbieux et al. 2018), we here put special emphasis on the discussion of particle size-based budgets for b_{bp} . These budgets are illustrated using the results obtained directly from our measurements (Fig. 6a) and after adjustment for imperfect size-fractionation (Fig. 6b), as described in “Methods” section.

Figure 6a suggests that the samples can be grouped into three categories based on the contribution of the small particle-size fraction to b_{bp} . The first group includes the four samples (P_N , P_M , O_S , and O_C) with the highest contribution of small particles as indicated by $b_{bps}/b_{bp} > 60\%$. The samples with b_{bp} most dominated by small particles are P_N and O_C with b_{bps}/b_{bp} around 80%. These samples are highly organic in nature with high values of POC/SPM, and are dominated by phytoplankton (Table 3). Interestingly, while P_N distinguishes itself in terms of the smallest values for particle size metrics, D_v^{50} and D_v^{90} , and hence the largest relative role of small-sized particles in the PSD, this feature is not observed in O_C (Table 3). We note that although the metrics of particulate composition, especially Chl a /SPM and a_{ph}/a_p , suggest a dominant role of phytoplankton, this result does not automatically imply that phytoplankton cells are the dominant direct source of backscattering in these samples. An important relevant point is that the abundance of nonalgal particles in seawater can often be higher compared with phytoplankton cells across the optically significant size range (Stramski and Kiefer 1991; Jonasz and Fournier 2007). Therefore, the question of partitioning backscattering between different types of particles cannot be unambiguously resolved without quantitative information on various properties, including the concentration and size distribution, of separate phytoplankton and nonalgal particulate components present in the samples. Such information is, however, beyond the reach of present experimental methods. Another organic-dominated sample in the first group, O_S , also has a high value of b_{bps}/b_{bp} above 70% but in this case, organic nonalgal particles are considerably more important than phytoplankton (Table 3). Finally, the fourth sample in the first group, P_M , with b_{bps}/b_{bp} of about 64% is more balanced in terms of organic and inorganic particulate matter as indicated by lower POC/SPM of 0.22; however, phytoplankton play a major role, especially in terms of high value of a_{ph}/a_p (Table 3). It is also remarkable that the values for particle size metrics, D_v^{50} and D_v^{90} , vary significantly among the four samples from this first group (Table 3). In summary, the results for this first group of samples indicate that particulate backscattering can be dominated by the small size fraction in samples that are characterized by quite different particulate compositions and size distributions.

The second group includes the samples with the lowest contribution of small particles, $b_{bps}/b_{bp} < 40\%$, and therefore highest combined contribution of medium and large particles. This group includes the two inorganic-dominated samples

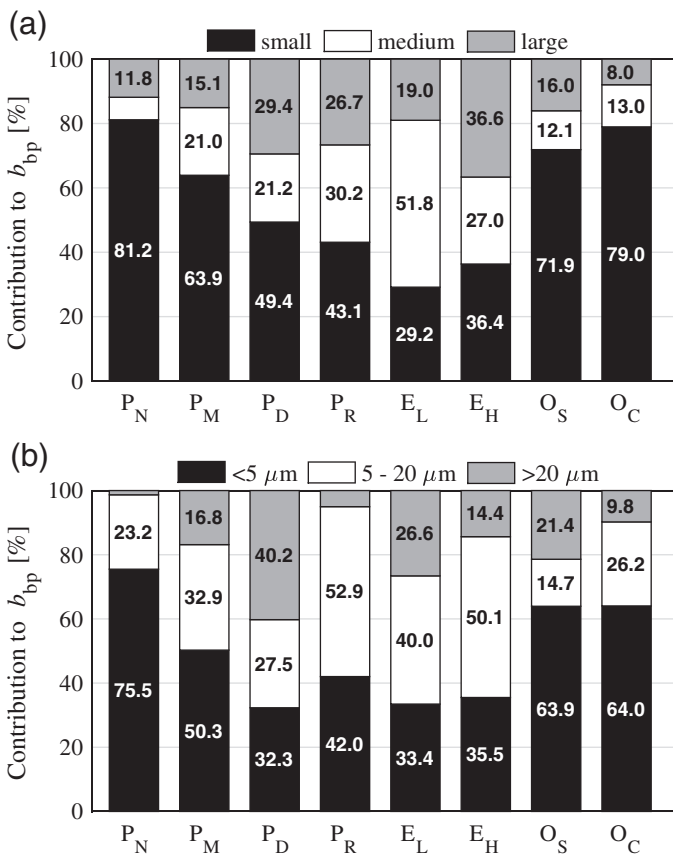


Fig. 6. (a) Particulate backscattering budget in terms of contributions of particle-size fractions to total particulate backscattering coefficient, b_{bp} , for the eight samples as indicated below each set of bars. Results for small, medium, and large particle-size fractions are shown as a percentage of total b_{bp} on the basis of measurements on original (unfiltered) and size-fractionated samples. (b) Same as panel (a) but results were obtained after adjustment for imperfect fractionation. Number values (in percentage) for the size fractions are displayed within the bar when possible.

collected in the San Diego River Estuary, E_L and E_H , which also exhibit the weakest role of phytoplankton among the examined samples. Because the particle size metrics for these two samples are quite different (Table 3), our results suggest that the scenario of relatively weak contribution of small particles to backscattering can occur in samples with significant differences in PSD. However, it is important to note that these two samples also differ in terms of the proportions of organic and inorganic particles both in the small particle-size fractions and original unfiltered samples (Table 3).

The third group includes the samples with intermediate, but still considerable contribution of small particles, $40\% < b_{bps}/b_{bp} < 50\%$, and accordingly, similar or somewhat larger combined contribution of medium and large particles. This group includes two samples from the SIO Pier with very different compositional characteristics, P_D and P_R . P_D was collected during enhanced presence of diatom *H. hauckii* and is apparently dominated by these large-sized microphytoplankton as corroborated by the highest values of particle size metrics, D_v^{50} and D_v^{90} , among all examined samples (Table 3). In contrast, P_R was collected after a rain event and is dominated by inorganic particles although phytoplankton appear to have a considerable presence in this sample. P_R has a value of D_v^{50} that is nearly threefold lower compared with P_D ; however, the difference for D_v^{90} is not as substantial between the two samples (Table 3).

Figure 6b shows that the particle size-based budget for backscattering coefficient after adjustment for imperfect size-fractionation is qualitatively similar to that based on measurements without adjustment. Specifically, the grouping of samples remains similar with P_N , P_M , O_S , and O_C still having the greatest role of small particles that are now defined more rigorously as particles $< 5 \mu\text{m}$ in size. For these samples, b_{bps}^*/b_{bp} ranges from about 50% to 75%. These percent contributions are, however, slightly lower compared with those based directly on size-fractionated measurements. The percent contributions of small particles to b_{bp} for E_L and E_H are still among the lowest (33–36%) in Fig. 6b, but in this case, the adjustment for imperfect fractionation has not resulted in consistent reduction of these contributions. For sample P_D , which is dominated by diatoms from microphytoplankton size range, this adjustment resulted in the most significant reduction of percent contribution of small particle-size fraction from about 49% (Fig. 6a) to 32% (Fig. 6b). Thus, in the adjusted budget, this sample along with E_L and E_H represents the weakest role of small particles in backscattering. For sample P_R , the adjustment for imperfect fractionation made no significant effect on the contribution of small-particle fraction to b_{bp} , which is about 42%.

The effects of adjustment for imperfect fractionation on the backscattering budget for the medium and large particle-size fractions, especially how the contributions are partitioned between these fractions, are more convoluted. In general, however, the adjustment resulted in an increase of the contribution

of medium-sized particles to b_{bp} for all samples except for E_H . With regard to the role of large particles $> 20 \mu\text{m}$ in size, the most noteworthy result is that the adjustment resulted in an increase of the contribution from about 29% to 40% for sample P_D . This result suggests that under conditions leading to an abundance of large-celled diatoms, the microphytoplankton size range can produce a very important contribution to particulate backscattering extending to, or perhaps even exceeding, 40%.

Figure 7 shows the particle size-based budgets in the same fashion as Fig. 6, except that it is for the particulate scattering coefficient, b_p . In agreement with data for $\beta_p(\psi)$ in Fig. 5, the results based on size-fractionated measurements in Fig. 7a show that small particle-size fraction is the most important contributor to b_p for all samples, except for E_L and E_H . The percent contributions of small particles to b_p in Fig. 7a are generally higher than or about the same as the corresponding contributions for b_{bp} in Fig. 6a. However, the adjustment for imperfect fractionation resulted in a significant decrease in the contribution of small-sized particles ($< 5 \mu\text{m}$) to b_p (Fig. 7b). For example, the contribution of small-sized particles to b_p decreased from 84% to 26% for sample O_C and from 71% to 40% for sample O_S . Similar decreases were observed for the other two samples that belong to the first group of samples (P_N and P_M), as described above in relation to the

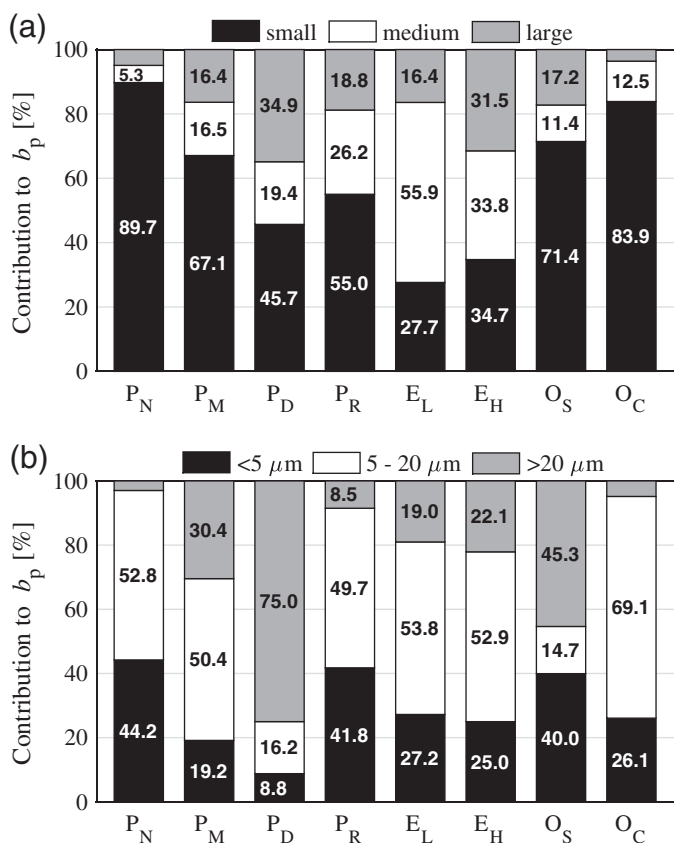


Fig. 7. Same as Fig. 6 but for the particulate scattering coefficient, b_p .

backscattering budget. As a result of adjustment for imperfect fractionation, the contribution of medium-sized particles to b_p increased for most samples, in some cases to values over 50% (P_N , P_M , and O_C). For a few samples (P_M , P_D , and O_S), this adjustment also resulted in considerable increase in the contribution of large-sized particles ($> 20 \mu\text{m}$) to b_p . In particular, for diatom-dominated sample P_D , the percent contribution increased more than twofold from about 35% (Fig. 7a) to 75% (Fig. 7b). The contribution of large-sized particles to b_p did not, however, increase for all samples and, in some cases, decreased slightly (P_R).

The patterns in Fig. 7 indicate that the particle size-based budget for b_p is considerably more sensitive to imperfect fractionation than the budget for b_{bp} (Fig. 6). This result is consistent with earlier modeling studies of light scattering by polydisperse particle assemblages, which indicated that the particle size-based contributions to b_p are more heavily weighted toward larger particles compared with contributions to b_{bp} (Stramski and Kiefer 1991). Accordingly, our data show that the adjustment for the presence of particles larger than $5 \mu\text{m}$ in the $5 \mu\text{m}$ filtrate has a greater effect on the b_p budget than the b_{bp} budget. As a result, while four out of eight samples exhibit the small-particle ($< 5 \mu\text{m}$) contributions to b_{bp} greater than 50% in the adjusted budget (Fig. 6b), all samples have contributions less than 45% to b_p (Fig. 7b). Along the same lines, while in the adjusted budgets, the highest large-particle ($> 20 \mu\text{m}$) contribution is about 40% for b_{bp} , it is 75% for b_p .

Although size-fractionated measurements and scattering computations to assess the effect of imperfect fractionation are unavoidably subject to some limitations, the combination of these results provided significant insights into the roles of particle size and composition in light scattering by particulate assemblages in seawater. Our study supports the notion that assemblages with contrasting particle size and compositional characteristics can produce very different scenarios for particulate scattering, b_p , and backscattering, b_{bp} budgets in terms of relative contributions of different particle-size fractions (Stramski et al. 2004). Our results also indicate that particle assemblages with contrasting characteristics can produce similar scenarios for particle size-based b_p and b_{bp} budgets.

Our results quantitatively demonstrate several highly different scenarios of particle size-based scattering budgets on the basis of analysis of eight contrasting samples from coastal environments, including nearshore samples dominated by organic particulate matter with predominant role of small-celled or large-celled phytoplankton, estuarine samples dominated by inorganic particles, and offshore samples representative of phytoplankton-dominated subsurface Chl *a* maximum and near-surface water dominated by organic nonalgal particles. Despite intricate interplay between the effects of particle size and composition on light scattering, we observed that small particles ($< 5 \mu\text{m}$ in size) consistently produced a major or dominant contribution to b_{bp} (close to or more than 50%) in organic, either phytoplankton or nonalgal, dominated samples in spite

of significant variations in particle size metrics between these samples. The notable exception was a sample dominated by large-celled diatoms from microphytoplankton size range, which exemplifies a specific scenario when large particles ($> 20 \mu\text{m}$) can play a considerable role in backscattering (about 40%). In addition, we observed a trend for inorganic-dominated samples exhibiting consistently lower contributions of small particles to b_{bp} (~ 30 – 40%). This trend for reduced contribution of small particles associated with inorganic-dominated assemblages having generally higher refractive index of particles, compared with organic-dominated assemblages with generally lower refractive index, is consistent with earlier predictions based on light scattering modeling of idealized populations of marine particles with low and high refractive index (Stramski and Kiefer 1991).

The chlorophyll *a* concentration in our coastal samples was $> 0.5 \text{ mg m}^{-3}$, so these samples are not representative of vast open-ocean areas where Chl *a* is typically $< 0.5 \text{ mg m}^{-3}$. Our two offshore samples (O_S and O_C) and the nearshore sample with the highest proportion of small particles (P_N) most closely resemble the characteristics of samples from open-ocean oligotrophic waters. For these three samples, the contribution to b_{bp} of particles $< 5 \mu\text{m}$ was estimated to range from 64% to 75%. Because the open-ocean oligotrophic samples are also expected to be organic-dominated with similar or perhaps even higher relative abundance of small particles, the contribution of small-sized particles to b_{bp} can also be expected to be similarly high or higher than our estimates for these three samples. Given such relatively high estimates of percent contributions for the size fraction $< 5 \mu\text{m}$, it is conceivable that very small particles from picoplankton and colloidal size range ($< 2 \mu\text{m}$) can play a major or dominant role in backscattering under nonbloom conditions in open-ocean waters. While this supposition is generally consistent with earlier theoretical and experimental results (Stramski and Kiefer 1991; Dall'Olmo et al. 2009; Organelli et al. 2018), it requires further research. There are also other related questions that are difficult to address but demand special attention in future research. For example, the role of phytoplankton cells as a direct source of backscattering vs. the role of coexisting nonalgal particles that are typically more abundant than phytoplankton, except perhaps for specific particle-size range under bloom conditions, is poorly understood. Another example is the need to consider the effects of variations in particle shape on light scattering by natural assemblages, which present particular challenges for theoretical and experimental studies and receive less attention that the effects associated with particle size and composition.

References

- Aas, E. 1996. Refractive index of phytoplankton derived from its metabolic composition. *J. Plankton Res.* **18**: 2223–2249. doi:10.1093/plankt/18.12.2223.
- Antoine, D., D. A. Siegel, T. S. Kostadinov, S. Maritorea, N. B. Nelson, B. Gentili, V. Vellucci, and N. Guillocheau. 2011.

- Variability in optical particle backscattering in contrasting bio-optical oceanic regimes. *Limnol. Oceanogr.* **56**: 955–973. doi:10.4319/lo.2011.56.3.0955.
- Babin, M., A. Morel, V. Fournier-Sicre, F. Fell, and D. Stramski. 2003. Light scattering properties of marine particles in coastal and open ocean waters as related to the particle mass concentration. *Limnol. Oceanogr.* **48**: 843–859. doi:10.4319/lo.2003.48.2.0843
- Balch, W. M., D. T. Drapeau, T. L. Cucci, R. D. Vaillancourt, K. A. Kilpatrick, and J. J. Fritz. 1999. Optical backscattering by calcifying algae: Separating the contribution by particulate inorganic and organic carbon fractions. *J. Geophys. Res.* **104**: 1541–1558. doi:10.1029/1998JC900035.
- Balch, W. M., D. Drapeau, J. Fritz, B. Bowler, and J. Nolan. 2001. Optical backscattering in the Arabian Sea: Continuous underway measurements of particulate inorganic and organic carbon. *Deep-Sea Res. Part I Oceanogr. Res. Pap.* **48**: 2423–2452. doi:10.1016/S0967-0637(01)00025-5.
- Barbieux, M., et al. 2018. Assessing the variability in the relationship between the particulate backscattering coefficient and the chlorophyll a concentration from a global Biogeochemical-Argo database. *J. Geophys. Res. Oceans* **123**: 1229–1250. doi:10.1002/2017JC013030.
- Boss, E., W. S. Pegau, W. D. Gardner, J. R. V. Zaneveld, A. H. Barnard, M. S. Twardowski, G. C. Chang, and T. D. Dickey. 2001. Spectral particulate attenuation and particle size distribution in the bottom boundary layer of a continental shelf. *J. Geophys. Res. Oceans* **106**: 9509–9516. doi:10.1029/2000JC900077.
- Boss, E., W. S. Pegau, M. Lee, M. Twardowski, E. Shybanov, G. Korotaev, and F. Baratange. 2004. Particulate backscattering ratio at LEO 15 and its use to study particle composition and distribution. *J. Geophys. Res.* **109**: C01014. doi:10.1029/2002JC001514.
- Carder, K. L., P. R. Betzer, and D. W. Eggimann. 1974. Physical, chemical, and optical measures of suspended-particle concentrations: Their intercomparison and application to the west African shelf, p. 173–193. *In* R. J. Gibbs [ed.], *Suspended solids in water*. Plenum Press. doi:10.1007/978-1-4684-8529-5_11
- Dall’Olmo, G., T. K. Westberry, M. J. Behrenfeld, E. Boss, and W. H. Slade. 2009. Significant contribution of large particles to optical backscattering in the open ocean. *Biogeosciences* **6**: 947–967. doi:10.5194/bg-6-947-2009.
- Davies, E. J., D. McKee, D. Bowers, G. W. Graham, and W. A. M. Nimmo-Smith. 2014. Optically significant particle sizes in seawater. *Appl. Opt.* **53**: 1067–1074. doi:10.1364/AO.53.001067.
- Gordon, H. R., O. B. Brown, and M. M. Jacobs. 1975. Computed relationships between the inherent and apparent optical properties of a flat homogeneous ocean. *Appl. Opt.* **14**: 417–427. doi:10.1364/AO.14.000417.
- Gordon, H. R., and A. Morel. 1983. Remote assessment of ocean color for interpretation of satellite visible imagery: A review. Springer-Verlag. doi:10.1007/978-1-4684-6280-7
- Gregg, W. W. 2002. Tracking the SeaWiFS record with a coupled physical/biogeochemical/ radiative model of the global oceans. *Deep-Sea Res. Part II Top. Stud. Oceanogr.* **49**: 81–105. doi:10.1016/S0967-0645(01)00095-9
- Gregg, W. W., and M. E. Conkright. 2002. Decadal changes in global ocean chlorophyll. *Geophys. Res. Lett.* **29**: 20-1–20-4. doi:10.1029/2002GL014689.
- Huot, Y., A. Morel, M. S. Twardowski, D. Stramski, and R. A. Reynolds. 2008. Particle optical scattering along a chlorophyll gradient in the upper layer of the eastern South Pacific Ocean. *Biogeosciences* **5**: 495–507. doi:10.5194/bg-5-495-2008.
- Jonasz, M., and G. Fournier. 2007. Light scattering by particles in water: Theoretical and experimental foundations. Elsevier.
- Kishino, M., M. Takahashi, N. Okami, and S. Ichimura. 1985. Estimation of the spectral absorption coefficients of phytoplankton in the sea. *Bull. Mar. Sci.* **37**: 634–642.
- Kitchen, J. C., and J. R. V. Zaneveld. 1992. A three-layered sphere model of the optical properties of phytoplankton. *Limnol. Oceanogr.* **37**: 1680–1690. doi:10.4319/lo.1992.37.8.1680.
- Koestner, D., D. Stramski, and R. A. Reynolds. 2018. Measurements of the volume scattering function and the degree of linear polarization of light scattered by contrasting natural assemblages of marine particles. *Appl. Sci.* **8**: 2690. doi:10.3390/app8122690.
- Kostadinov, T. S., D. A. Siegel, and S. Maritorea. 2009. Retrieval of the particle size distribution from satellite ocean color observations. *J. Geophys. Res.* **114**: C09015. doi:10.1029/2009JC005303.
- Li, L., D. Stramski, and R. A. Reynolds. 2014. Characterization of the solar light field within the ocean mesopelagic zone based on radiative transfer simulations. *Deep-Sea Res. Part I Oceanogr. Res. Pap.* **87**: 53–69. doi:10.1016/j.dsr.2014.02.005.
- Logan, B. E. 1993. Theoretical analysis of size distributions determined with screens and filters. *Limnol. Oceanogr.* **38**: 372–381. doi:10.4319/lo.1993.38.2.0372.
- Meyer, R. A. 1979. Light scattering from biological cells: Dependence of backscatter radiation on membrane thickness and refractive index. *Appl. Opt.* **18**: 585–588. doi:10.1364/AO.18.000585.
- Mobley, C. D. 1994. *Light and water: Radiative transfer in natural waters*. Academic Press.
- Mobley, C. D., L. K. Sundman, and E. Boss. 2002. Phase function effects on oceanic light fields. *Appl. Opt.* **41**: 1035–1050. doi:10.1364/AO.41.001035.
- Mobley, C. D., F. Chai, P. Xiu, and L. K. Sundman. 2015. Impact of improved light calculations on predicted phytoplankton growth and heating in an idealized upwelling-downwelling channel geometry. *J. Geophys. Res. Oceans* **120**: 875–892. doi:10.1002/2014JC010588.
- Morel, A. 1973. Diffusion de la lumière par les eaux de mer; résultats expérimentaux et approche théorique, p. 3.1-1–3.1-76. *In* *Optics of the sea*. AGARD Lecture series, No. **61**.

- Morel, A., and L. Prieur. 1977. Analysis of variations in ocean color. *Limnol. Oceanogr.* **22**: 709–722. doi:10.4319/lo.1977.22.4.0709.
- Morel, A., and A. Bricaud. 1986. Inherent optical properties of algal cells including picoplankton: Theoretical and experimental results. *Can. Bull. Fish. Aquat. Sci.* **214**: 521–559.
- Neukermans, G., H. Loisel, X. Meriaux, R. Astoreca, and D. McKee. 2012. In situ variability of mass-specific beam attenuation and backscattering of marine particles with respect to particle size, density, and composition. *Limnol. Oceanogr.* **57**: 124–144. doi:10.4319/lo.2011.57.1.0124.
- Neukermans, G., R. A. Reynolds, and D. Stramski. 2016. Optical classification and characterization of marine particle assemblages within the western Arctic Ocean. *Limnol. Oceanogr.* **61**: 1472–1494. doi:10.1002/lno.10316.
- Organelli, E., et al. 2017. Two databases derived from BGC-Argo float measurements for marine biogeochemical and bio-optical applications. *Earth Syst. Sci. Data* **9**: 861–880. doi:10.5194/essd-9-861-2017.
- Organelli, E., G. Dall’Olmo, R. J. W. Brewin, G. A. Tarran, E. Boss, and A. Bricaud. 2018. The open-ocean missing backscattering is in the structural complexity of particles. *Nat. Commun.* **9**: 5439. doi:10.1038/s41467-018-07814-6.
- Parsons, T. R., Y. Maita, and C. M. Lalli. 1984. A manual of chemical and biological methods for seawater analysis. Elsevier.
- Reynolds, R. A., D. Stramski, V. M. Wright, and S. B. Woźniak. 2010. Measurements and characterization of particle size distributions in coastal waters. *J. Geophys. Res.* **115**: C08024. doi:10.1029/2009JC005930.
- Reynolds, R. A., D. Stramski, and G. Neukermans. 2016. Optical backscattering by particles in Arctic seawater and relationships to particle mass concentration, size distribution, and bulk composition. *Limnol. Oceanogr.* **61**: 1869–1890. doi:10.1002/lno.10341.
- Ritchie, R. J. 2008. Universal chlorophyll equations for estimating chlorophylls a, b, c, and d and total chlorophylls in natural assemblages of photosynthetic organisms using acetone, methanol, or ethanol solvents. *Photosynthetica* **46**: 115–126. doi:10.1007/s11099-008-0019-7.
- Röttgers, R., and S. Gehnke. 2012. Measurement of light absorption by aquatic particles: Improvement of the quantitative filter technique by use of an integrating sphere approach. *Appl. Opt.* **51**: 1336–1351. doi:10.1364/AO.51.001336.
- Sheldon, R. W. 1972. Size separation of marine seston by membrane and glass-fiber filters. *Limnol. Oceanogr.* **17**: 494–498. doi:10.4319/lo.1972.17.3.0494.
- Slade, W. H., and E. Boss. 2015. Spectral attenuation and backscattering as indicators of average particle size. *Appl. Opt.* **54**: 7264–7277. doi:10.1364/AO.54.007264.
- Sparks, T., and G. Chase. 2015. Filters and filtration handbook, 6th ed. Elsevier.
- Stramski, D., and D. A. Kiefer. 1991. Light scattering by microorganisms in the open ocean. *Prog. Oceanogr.* **28**: 343–383. doi:10.1016/0079-6611(91)90032-H.
- Stramski, D., R. A. Reynolds, M. Kahru, and B. G. Mitchell. 1999. Estimation of particulate organic carbon in the ocean from satellite remote sensing. *Science* **285**: 239–242. doi:10.1126/science.285.5425.239.
- Stramski, D., A. Bricaud, and A. Morel. 2001. Modeling the inherent optical properties of the ocean based on the detailed composition of planktonic community. *Appl. Opt.* **40**: 2929–2945. doi:10.1364/AO.40.002929.
- Stramski, D., E. S. Boss, D. J. Bogucki, and K. J. Voss. 2004. The role of seawater constituents in light backscattering in the ocean. *Prog. Oceanogr.* **61**: 27–56. doi:10.1016/j.pocean.2004.07.001.
- Stramski, D., and others. 2008. Relationships between the surface concentration of particulate organic carbon and optical properties in the eastern South Pacific and eastern Atlantic Oceans. *Biogeosciences* **5**: 171–201. doi:10.5194/bg-5-171-2008.
- Stramski, D., R. A. Reynolds, S. Kaczmarek, J. Uitz, and G. Zheng. 2015. Correction of pathlength amplification in the filter-pad technique for measurements of particulate absorption coefficient in the visible spectral region. *Appl. Opt.* **54**: 6763–6782. doi:10.1364/AO.54.006763.
- Sullivan, J. M., and M. S. Twardowski. 2009. Angular shape of the oceanic particulate volume scattering function in the backward direction. *Appl. Opt.* **48**: 6811–6819. doi:10.1364/AO.48.006811.
- Twardowski, M. S., E. Boss, J. B. Macdonald, W. S. Pegau, A. H. Barnard, and J. R. V. Zaneveld. 2001. A model for estimating bulk refractive index from the optical backscattering ratio and the implications for understanding particle composition in case I and case II waters. *J. Geophys. Res.* **106**: 14129–14142. doi:10.1029/2000JC000404.
- Twardowski, M., and A. Tonizzo. 2018. Ocean color analytical model explicitly dependent on the volume scattering function. *Appl. Sci.* **8**: 2684. doi:10.3390/app8122684.
- van de Hulst, H. C. 1981. Light scattering by small particles. John Wiley & Sons.
- van der Linde, D. W. 1998. Protocol for the determination of total suspended matter in oceans and coastal zones. Technical Note I.98.182. Joint Research Centre.
- Whitmire, A. L., W. S. Pegau, L. Karp-Boss, E. Boss, and T. J. Cowles. 2010. Spectral backscattering properties of marine phytoplankton cultures. *Opt. Express* **18**: 15073–15093. doi:10.1364/OE.18.015073.
- Woźniak, S. B., and D. Stramski. 2004. Modeling the optical properties of mineral particles suspended in seawater and their influence on ocean reflectance and chlorophyll estimation from remote sensing algorithms. *Appl. Opt.* **43**: 3489–3503. doi:10.1364/AO.43.003489.
- Woźniak, S. B., D. Stramski, M. Stramska, R. A. Reynolds, V. M. Wright, E. Y. Miksic, M. Cichocka, and A. M. Cieplak. 2010.

- Optical variability of seawater in relation to particle concentration, composition, and size distribution in the nearshore marine environment at Imperial Beach, California. *J. Geophys. Res.* **115**: C08027. doi:[10.1029/2009JC005554](https://doi.org/10.1029/2009JC005554).
- Xu, G., B. Sun, S. D. Brooks, P. Yang, G. W. Kattawar, and X. Zhang. 2017. Modeling the inherent optical properties of aquatic particles using an irregular hexahedral ensemble. *J. Quant. Spectrosc. Radiat. Transf.* **191**: 30–39. doi:[10.1016/j.jqsrt.2017.01.020](https://doi.org/10.1016/j.jqsrt.2017.01.020).
- Zaneveld, J. R. V. 1995. A theoretical derivation of the dependence of the remotely sensed reflectance on the inherent optical properties. *J. Geophys. Res.* **100**: 13135–13142. doi:[10.1029/95JC00453](https://doi.org/10.1029/95JC00453).
- Zaneveld, J. R. V., D. M. Roach, and H. Pak. 1974. The determination of the index of refraction distribution of oceanic particulates. *J. Geophys. Res.* **79**: 4091–4095. doi:[10.1029/JC079i027p04091](https://doi.org/10.1029/JC079i027p04091).
- Zhang, X., Y. Huot, D. J. Gray, A. Weidemann, and W. J. Rhea. 2013. Biogeochemical origins of particles obtained from the inversion of the volume scattering function and spectral absorption in coastal waters. *Biogeosciences* **10**: 6029–6043. doi:[10.5194/bg-10-6029-2013](https://doi.org/10.5194/bg-10-6029-2013).

Acknowledgments

We acknowledge Eric Chen, Linhai Li, and Hugh Runyan for assistance during measurements and processing of data. We thank Xiaodong Zhang for providing software to calculate light scattering by hexahedrally shaped particles and to extrapolate backscattering measurements, and Wayne Slade for discussions regarding the LISST-VSF instrument. We also thank two anonymous reviewers for valuable comments on the manuscript. POC analysis of seawater samples was done at the Marine Science Institute, University of California Santa Barbara. This work was supported by NASA Terrestrial Hydrology and Ocean Biology and Biogeochemistry Programs (Grants NNX13AN72G and 80NSSC18K0956) and the NASA Earth and Space Science Fellowship Program (Grant NNX14AK93H).

Conflict of Interest

None declared.

Submitted 05 May 2019

Revised 24 June 2019

Accepted 27 June 2019

Associate editor: David Antoine